Supporting Information

Excellent Electrocatalytic Performance of Metal-free Thiophene-Sulfur Covalent Organic Framework for Hydrogen Evolution in Alkaline Medium

Yunchao Ma,[a,1] Yue Fu,[a,1] Wei Jiang[b], Yuanyuan Wu[b], Chunbo Liu, [*a,b] , Guangbo Che[*c]

and Qianrong Fang[*d]

[a]*Key Laboratory of Preparation and Application of Environmental Friendly Materials (Jilin Normal University), Ministry of Education, Changchun, 130103, P.R. China*

[b]*College of Environmental Science and Engineering, Jilin Normal University, Siping, 136000, P.R. China*

[c]*College of Chemistry, Baicheng Normal University, Baicheng, 137000, China*

[d]*State Key Laboratory of Inorganic Synthesis and Preparative Chemistry, Jilin University, Changchun 130012, China*

Table of contents

Section S1. Materials and characterization

S1.1 Materials and instruments

All starting materials and solvents, unless otherwise noted, were obtained from J&K scientific LTD. 2,2'-bithiophenyl-5,5'-dicarbaldehyde (bTDC) were purchased from Shanghai Aladdin Biochemical Technology Co.. Fourier transform infrared (FT-IR) spectra were acquired on a Thermoscientific Nicolet 4700 Fourier Transform Infrared Spectrometer with KBr pellet. Thermogravimetric analysis (TGA) was recorded on a STA 449 F3 *Jupiter* thermal analyzer with N_2 flow rate of 20 mL min^{-1} at a heating rate of 5 °C min^{-1} to 800 °C. PXRD data were collected on a PANalytical B.V. Empyrean powder diffractometer using a Cu Kα source (λ = 1.5418 Å) over the range of 2θ = 2.0−40.0° with a step size of 0.02° and 2 s per step. The sorption isotherm for N_2 was measured by using a Micromeritics ASAP 2460 analyzer with ultra-high-purity gas (99.999% purity). To estimate the pore size distributions, nonlocal density functional theory (NLDFT) was applied to analyze the N_2 isotherm on the basis of the model of N_2@77K on carbon with slit pores and the method of non-negative regularization. The SEM images were obtained on JEOL 8100 scanning electron microscope. X-ray photoelectron spectroscopy (XPS) was obtained by Escalab 250XI X-ray electron spectrometer (VG Scientific, America).

S1.2 Electrochemical measurements

The electrocatalytic properties of the catalysts for hydrogen evolution reaction were evaluated with a three-electrode configuration on a CHI 760E electrochemical workstation (CHI Instruments, Shanghai, China). To prepare the working electrode, 2 mg of the electrocatalyst combined with 600 μL of ethanol and 4 μL of Nafion was treated by ultrasonication for 20 min; then, the as-prepared suspension (12 μL, corresponding to a mass loading of 0.57 mg cm^{-2}) was slowly deposited on glassy carbon (GC, 3 mm diameter) electrode. After continuous purging with N_2 to remove dissolved gases, 1.0 M KOH, 0.5 M H_2SO_4 and 1.0 M PBS solutions were used as alkaline, acidic and neutral electrolytes, respectively. The as-prepared sample was directly used as the working electrode. Hg/HgO and graphite rods were used as reference and counter electrodes in 1.0 M KOH and 1.0 M PBS solutions. Potential measurements were all converted to potential values

relative to the reversible hydrogen electrode (RHE) based on $E_{(vs.\ RHE)} = E_{(vs.\ Hg/HgO)} + 0.0591*pH + 0.098$. While Saturated Ag/AgCl in 0.5 M H_2SO_4 was used as the reference electrode, Pt filaments were used as counter electrodes. the potentials were corrected to the reversible hydrogen electrode (RHE) in accordance $E_{(vs.\ RHE)} = E_{(vs.\ Ag/AgCl)} + 0.059*pH + 0.197$. LSV curves were obtained in a nitrogen-saturated electrolyte at a sweep rate of 10 mV/s. The ohmic potential drop (iR) losses that arise from the solution resistance were all corrected. The EIS was tested in the constant potential mode in the frequency range 1 Hz to 100 kHz. Cyclic voltammetry (CV) curves of the samples in different electrolytes were tested at different scan rates (20, 40, 60, 80 and 100 mV/s) and further calculated to obtain the bilayer capacitance value C_{dl}.

S1.3 The HER reaction process

In alkaline medium, the HER reaction process is assigned to the Volmer-Heyrovsky pathway[1,2]. Electrochemical reaction step:

$$H^* + e^- \rightarrow H_{ads} \qquad \text{Volmer reaction step}$$

$$H^* + H_{ads} + e^- \rightarrow H_2 \qquad \text{Heyrovsky reaction step}$$

$$2H_{ads} \rightarrow H_2 \qquad \text{Tafel reastion step}$$

Where H* represents the catalytic site with an adsorbed H-species.

S1.4 The Tafel equation is presented as:

$$\eta = a + b \log(i/i_0)$$

η is the overpotential, i is current density, i_0 is the exchange current density, b is the Tafel slope and a is the constant term.

S1.5 The HER reaction rate-limiting step

In these multi-step reactions, the Tafel slope is $b = 2.303\ RT/\alpha F$, where b is the Tafel slope (V), R the gas constant (J K^{-1} mol^{-1}), T temperature (K), α the transfer coefficient (independent of temperature) and F is the Faraday constant (C mol^{-1}). The Tafel slope plays an important role in demonstrating the mechanism when the mechanism is the rate-determining step (rds) of a multi-

step reaction[3]. The widely accepted view is that it has been widely accepted that the value of the charge-transfer coefficient, depends on the rds for multi-step reactions.

When the rds is Volmer step or Volmer step + Heyrovsky step or Volmer step + Tafel step, the value of $\alpha = 0.5$, the Tafel slope becomes 118 mV dec^{-1} at 298 K calculated from $b = 2.303\ RT/\alpha F$. Other possibilities are $\alpha = 1.5$ and b = 40 mV when the Heyrovsky step is the rds, and $\alpha = 2$ and b = 30 mV when the Tafel step is the rds[4]. Therefore, the Tafel slopes and the α values are b = 131 mV and $\alpha = 0.45$ for the JLNU-301 electrode, b = 113 mV and $\alpha = 0.52$ for the JLNU-302 electrode.

S1.6 Electrochemical active surface area (ECSA) calculation:

The double layer capacitance (C_{dl}) was evaluated according to the following equation: $C_{dl} = \Delta j/v$, which Δj is the current density difference between anode and cathode at the potential corresponding to 0.25 V and v is the scan rate. The slope of the line plots corresponds to the double of C_{dl}. Subsequently, the ECSA was estimated from the C_{dl} according to ECSA= C_{dl}/C_s, which C_s is the specific capacitance.

S1.7 Faraday efficiency calculation:

The Faraday efficiency calculation: $FE\% = \frac{(\text{Amount of } H_2 \text{ generated experimentally})}{(\text{Amount of } H_2 \text{ generated theoretically})} = \frac{nNF}{Q} \times 100\%$

Where n equals to 2, N is the number of hydrogen produced during the experiment (mol) and Q is the total charge passed through the reaction.

S1.8 Synthesis of JLUN-301

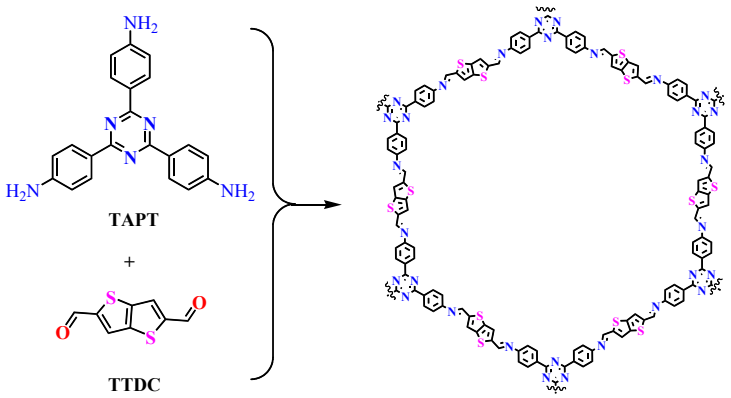

2,4,6-tris(4-aminophenyl)-1,3,5-triazine (TAPT) (0.04 mmol, 14.18 mg) and Thieno[3,2-b]thiophene-2,5-dicarboxaldehyde (TTDC) (0.06 mmol, 11.78 mg) were weighted into a Pyrex tube (volume: *ca* 20 ml with a both length of 10 cm, neck length of 9 cm) and to the mixture was added mesitylene (0.75 ml), 1,4-dioxane(0.25 ml) and 0.1 ml of aqueous acetic acid (6.0 mol/L). The tube was flash frozen at 77 K (LN_2 bath), evacuated to an internal pressure of 0.15 mmHg and flame sealed. Upon sealing the length of the tube was reduced to *ca*. 13 cm. The reaction mixture was heated at 120 ℃ for 72 h to afford a orange precipitate which was isolated by filtration over a medium glass frit and washed with anhydrous acetone (3 × 20 ml). The yield is about 74.0% (19.2 mg). The solvent was removed under vacuum at 80 ℃ to afford the corresponding products as orange powder of JLNU-301. Anal. Calcd for $C_{66}H_{36}N_{12}S_6$: C: 66.67; H: 3.03; N:14.14; S: 16.16. Found: C:66.58; H: 3.11; N: 14.08; S: 16.23. Solid-state ^{13}C NMR (500MH_Z): 13.11, 18.38, 57.96, 106.75, 114.99, 129.14, 133.99, 142.79, 150.81, 169.07 ppm. FT-IR (KBr): 810, 880, 1052, 1092, 1460, 1578, 1613, 2968, 3398 cm^{-1}.

S1.9 Synthesis of JLUN-302

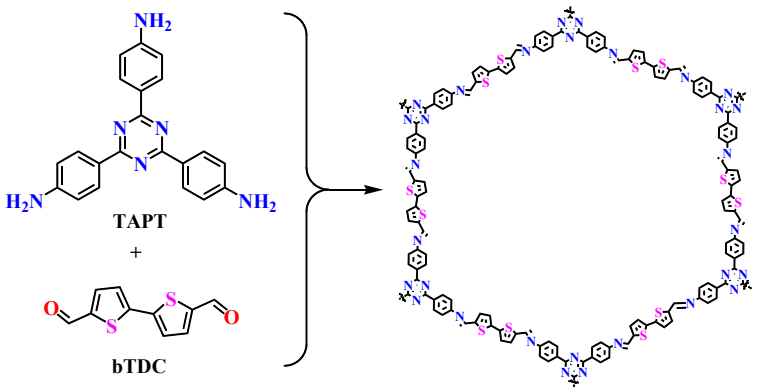

In a similar procedure of JLNU-301, 2,4,6-tris(4-aminophenyl)-1,3,5-triazinez (TAPT) (0.03 mmol, 10.63 mg) and 2,2'-dithiophene-5,5'-dicarboxaldehyde (bTDC) (0.045 mmol, 10.00 mg) were weighted into a Pyrex tube (volume: *ca* 20 ml with a both length of 10 cm, neck length of 9 cm) and to the mixture was added butanol (1 ml) and 0.1 ml of aqueous acetic acid (6.0 mol/L). The tube was flash frozen at 77 K (LN_2 bath), evacuated to an internal pressure of 0.15 mmHg and flame sealed. Upon sealing the length of the tube was reduced to *ca.* 13 cm. The reaction mixture was heated at 120 ℃ for 72 h to afford a orange precipitate which was isolated by filtration over a medium glass frit and washed with anhydrous acetone (3 × 20 ml). The yield is about 72.3% (15.2 mg). The solvent was removed under vacuum at 80 ℃ to afford the corresponding products as red powder for JLNU-302. Anal. Calcd for $C_{72}H_{42}N_{12}S_6$: C: 68.25; H: 3.32; N: 13.27; S: 15.16. Found: C: 68.31; H: 3.27; N: 13.25; S: 15.17. Solid-state ^{13}C NMR ($500MH_Z$): 18.71, 25.67, 33.58, 114.37, 117.27, 130.46, 133.89, 142.59, 152.07, 170.04, 182.31 ppm. FT-IR (KBr): 806, 868, 1048, 1362, 1502, 1574, 1613, 2324, 3680 cm^{-1}.

Section S2: PXRD patterns

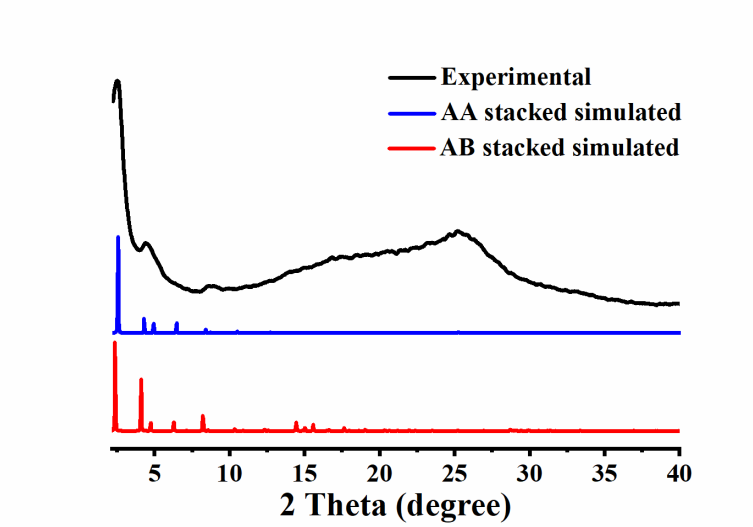

Figure S1. Comparison of PXRD patterns for JLNU-301: calculated based on the AA stacked (blue), AB stacked (red), and experiment (black).

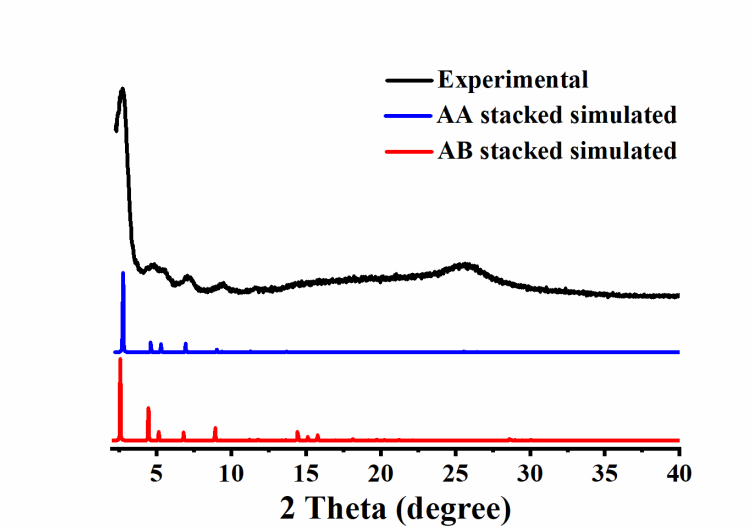

Figure S2. Comparison of PXRD patterns for JLNU-302: calculated based on the AA stacked (blue), AB stacked (red), and experiment (black).

Section S3: TGA

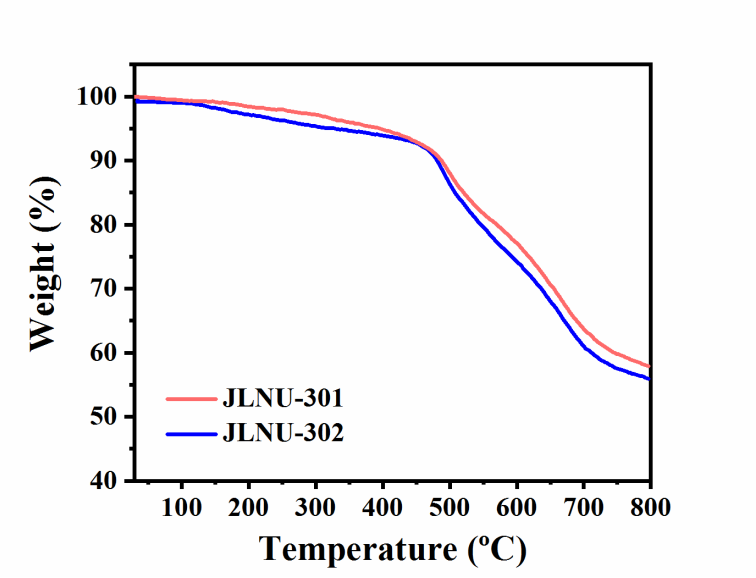

Figure S3. TGA curves of JLNU-301 and JLNU-302 in N_2 atmosphere.

Section S4: Gas adsorption isotherms

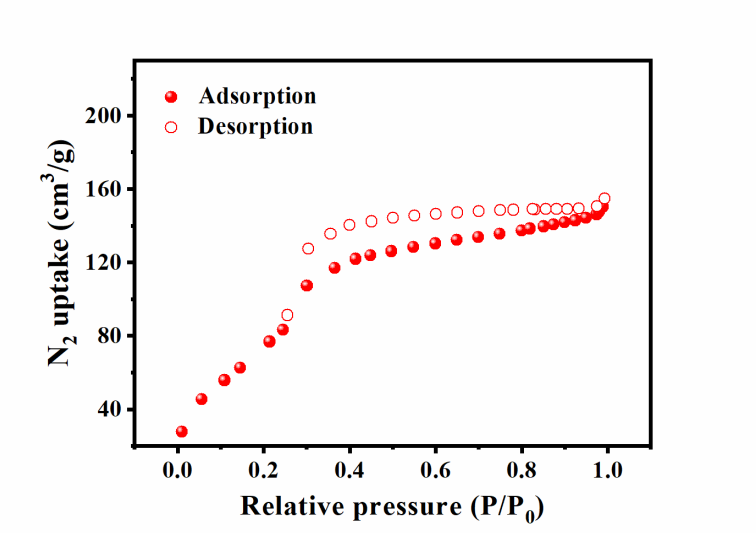

Figure S4. N_2 adsorption-desorption isotherms of JLNU-301.

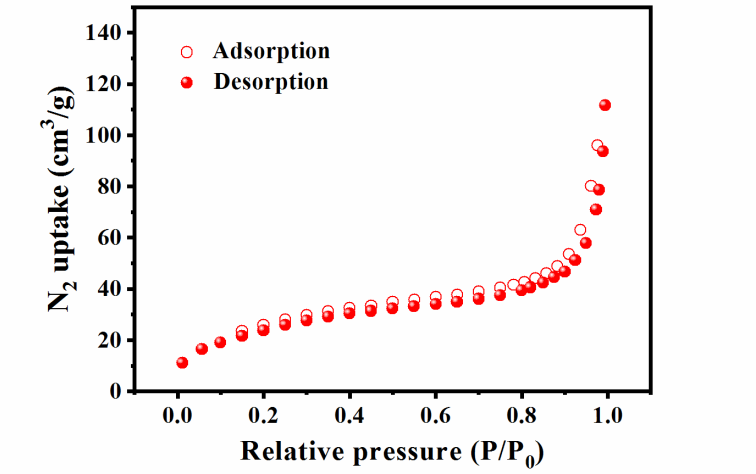

Figure S5. N_2 adsorption-desorption isotherms of JLNU-302.

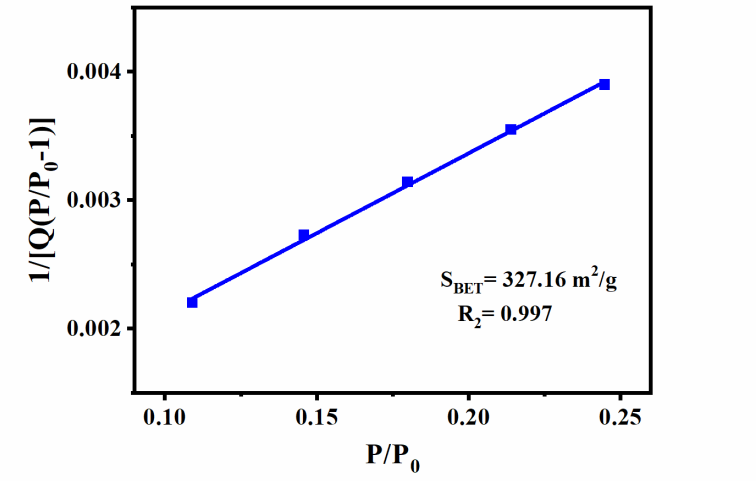

Figure S6. BET pole of JLNU-301 calculated from N_2 adsorption isotherm at 77 K.

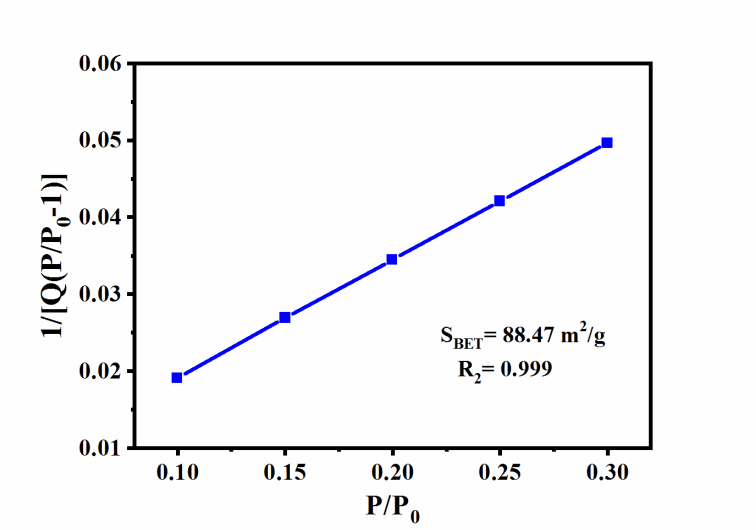

Figure S7. BET pole of JLNU-302 calculated from N_2 adsorption isotherm at 77 K.

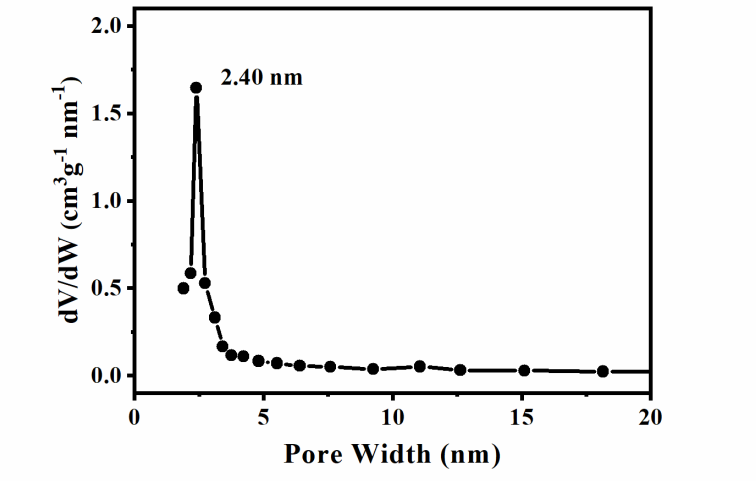

Figure S8. The pore size distribution curve of JLNU-301.

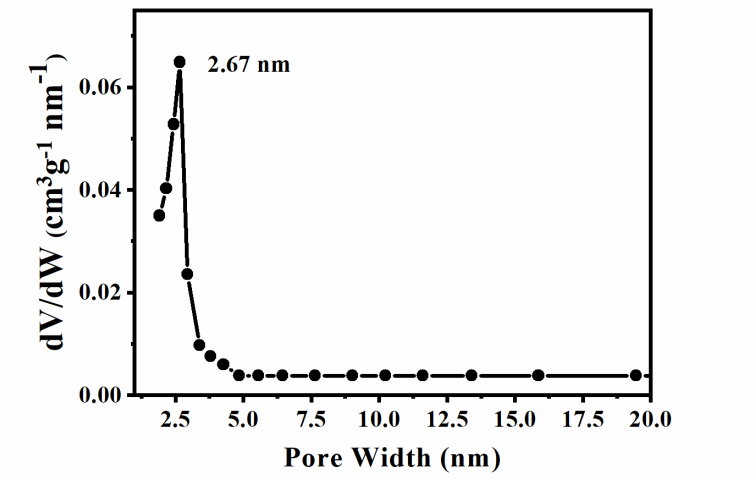

Figure S9. The pore size distribution curve of JLNU-302.

Section S5: Stability test

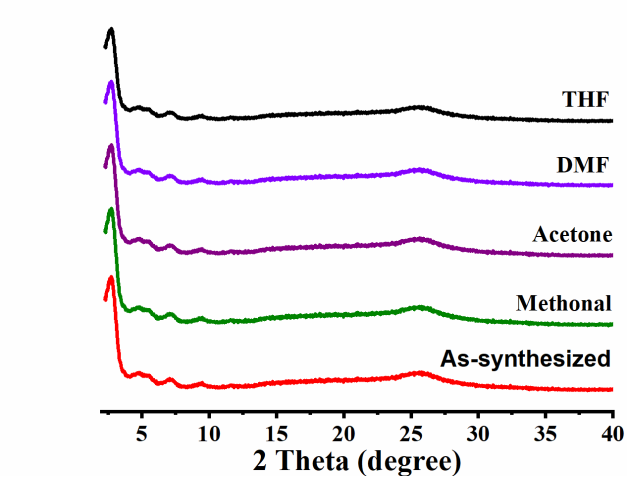

Figure S10. PXRD patterns of JLNU-301 after 3 d treatment in different organic solvents.

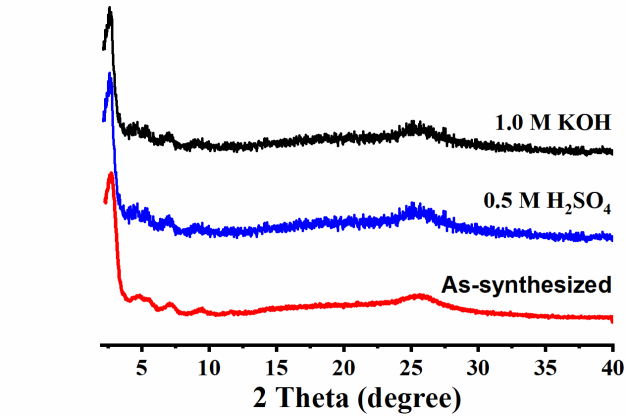

Figure S11. PXRD patterns of JLNU-301 after 3 d treatment in acid/base aqueous solutions.

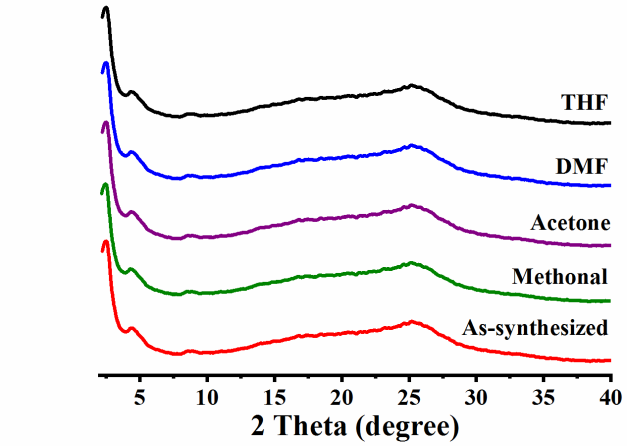

Figure S12. PXRD patterns of JLNU-302 after 3 d treatment in different organic solvents.

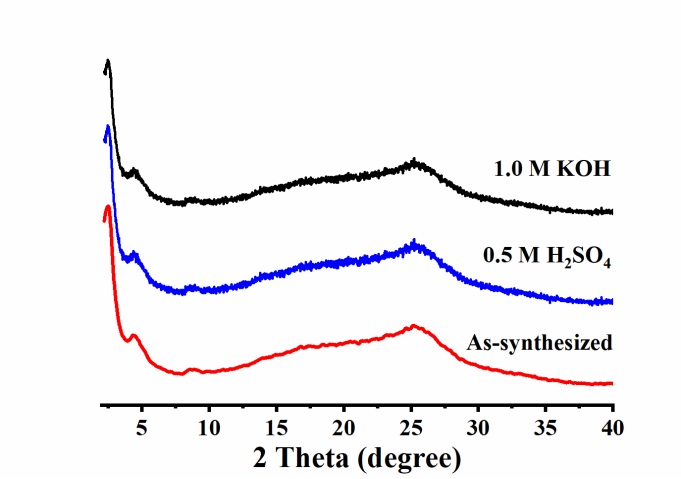

Figure S13. PXRD patterns of JLNU-302 after 3 d treatment in acid/base aqueous solutions.

Section S6: Structure and composition of JLNU-COFs after HER stability test

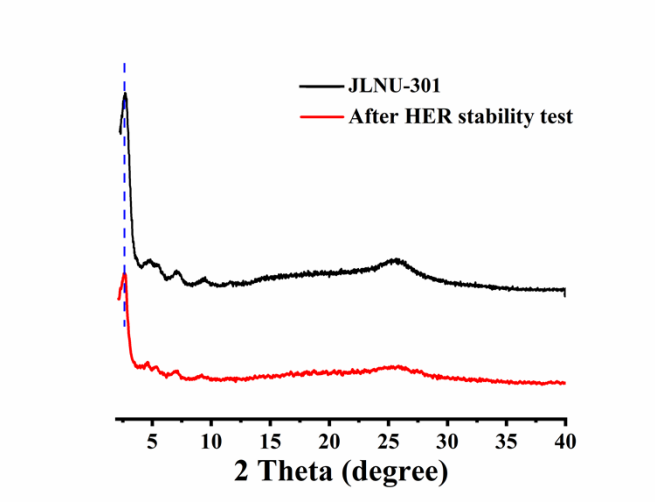

Figure S14. PXRD of JLNU-301 before and after 20 hours of HER stability test.

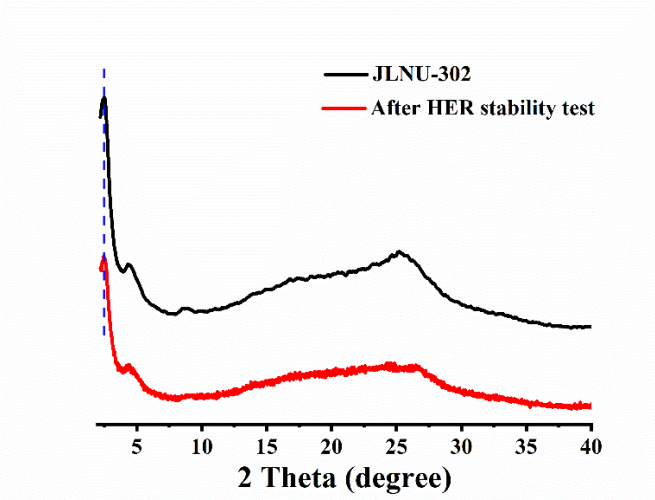

Figure S15. PXRD of JLNU-302 before and after 20 hours of HER stability test.

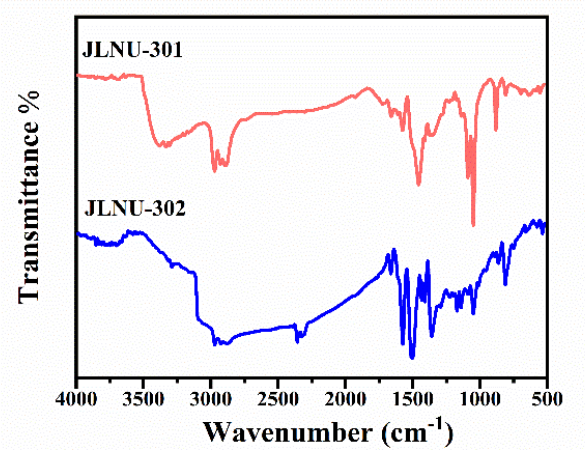

Figure S16. FT-IR of JLNU-COFs before and after 20 hours of HER stability test.

Section S7: Electrochemical performance

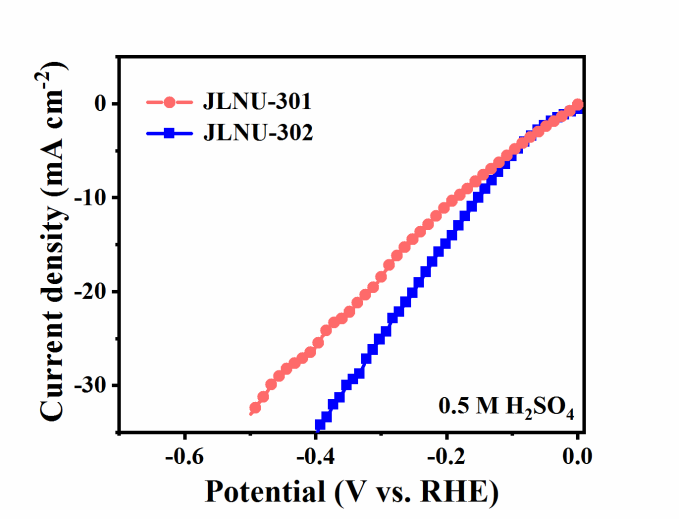

Figure S17. Polarization curves of JLNU-301 and JLNU-302 in 0.5 M H_2SO_4.

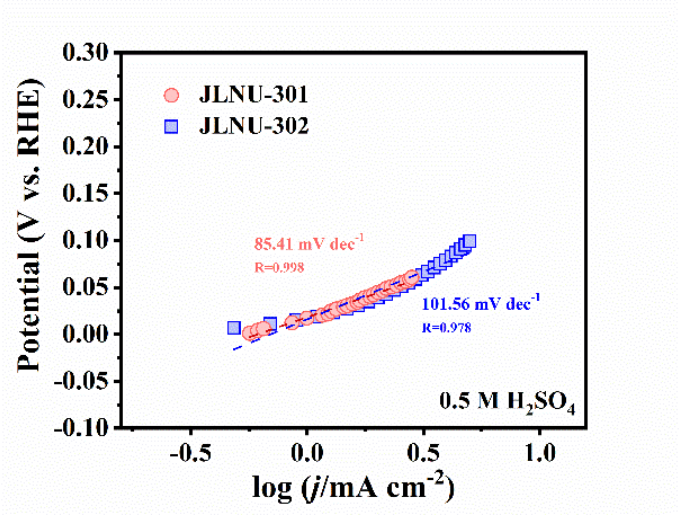

Figure S18. Tafel plots of JLNU-301 and JLNU-302 in 0.5 M H_2SO_4.

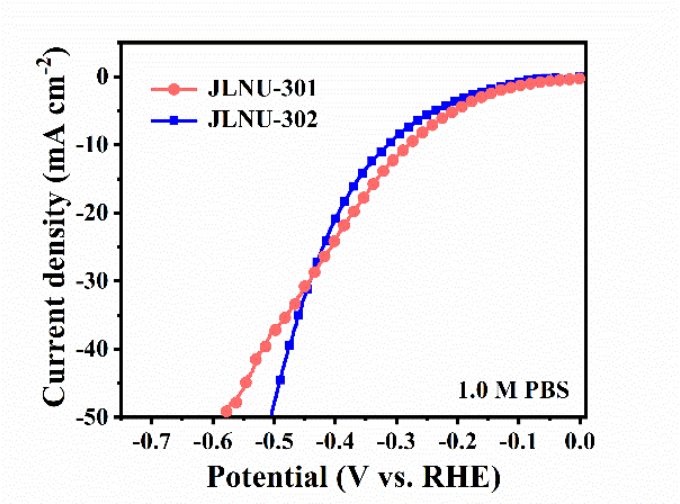

Figure S19. Polarization curves of JLNU-301 and JLNU-302 in 1.0 M PBS.

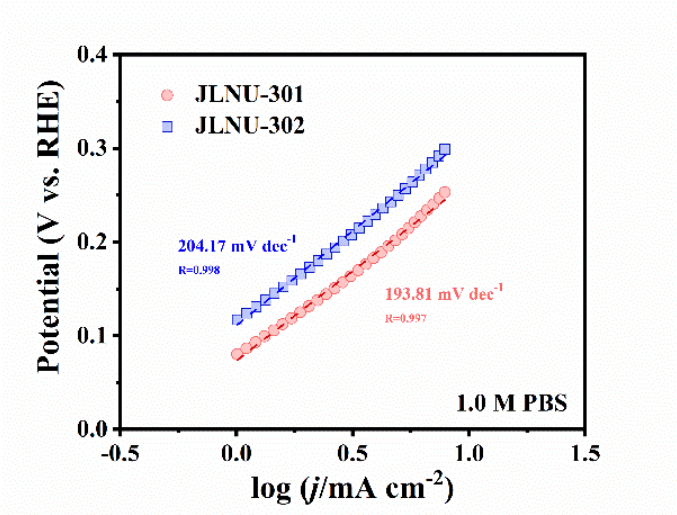

Figure S20. Tafel plots of JLNU-301 and JLNU-302 in 1.0 M PBS.

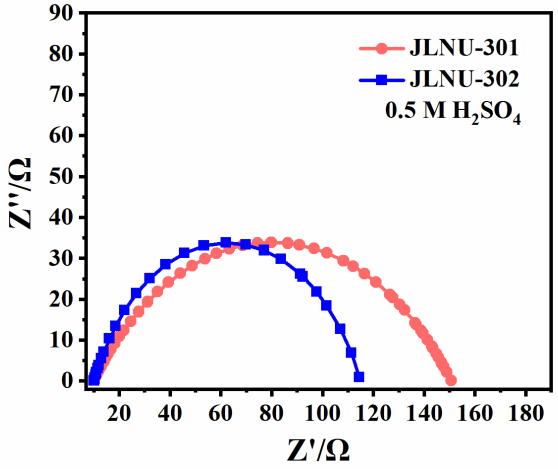

Figure S21. The Nyquist plots of JLNU-301 and JLNU-302 at 0.5 M H_2SO_4.

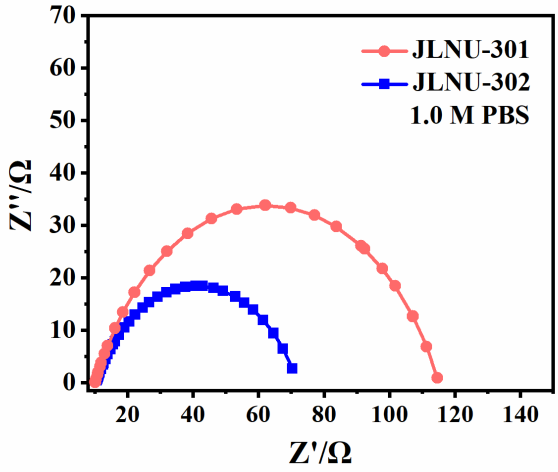

Figure S22. The Nyquist plots of JLNU-301 and JLNU-302 at 1.0 M PBS.

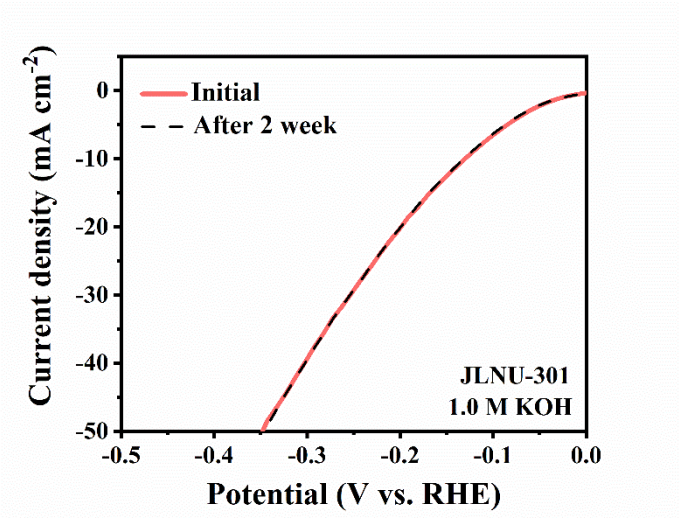

Figure S23. The LSV curves of JLUN-301 before and after 2-week tests.

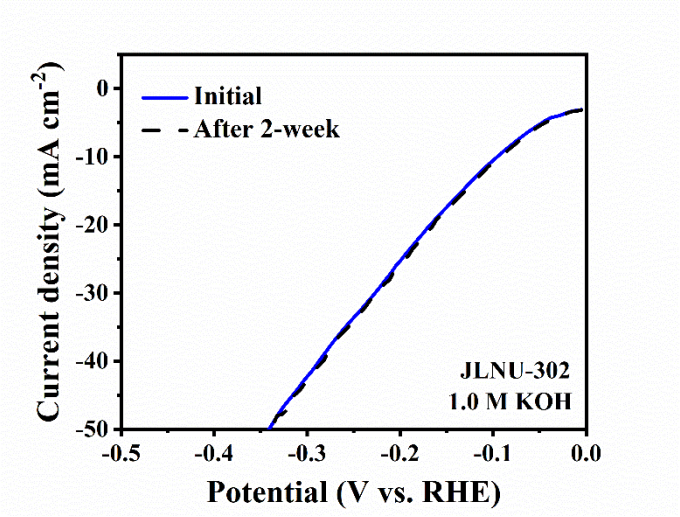

Figure S24. The LSV curves of JLUN-302 before and after 2-week tests.

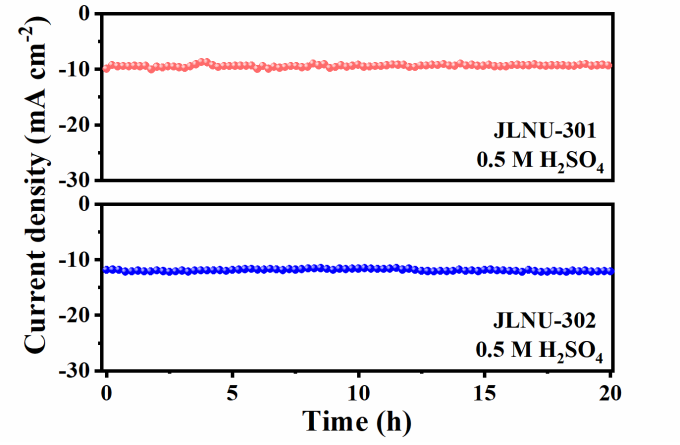

Figure S25. Chronopotentiometry plot for JLNU-301 and JLNU-302 in 0.5 H_2SO_4.

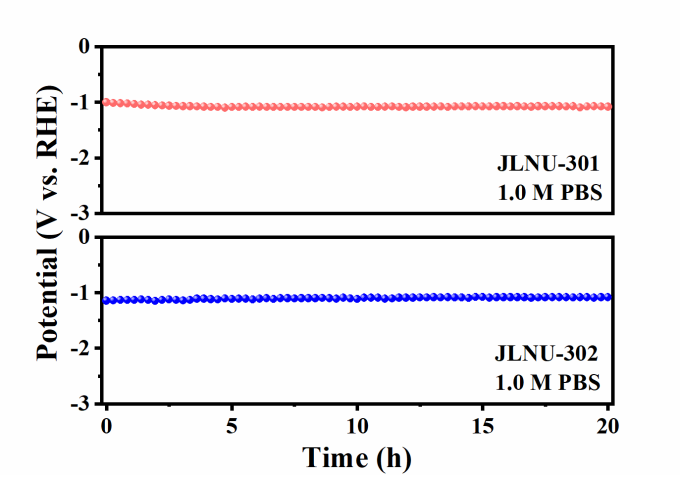

Figure S26. Chronopotentiometry plot for JLNU-301 and JLNU-302 in 1.0 M PBS.

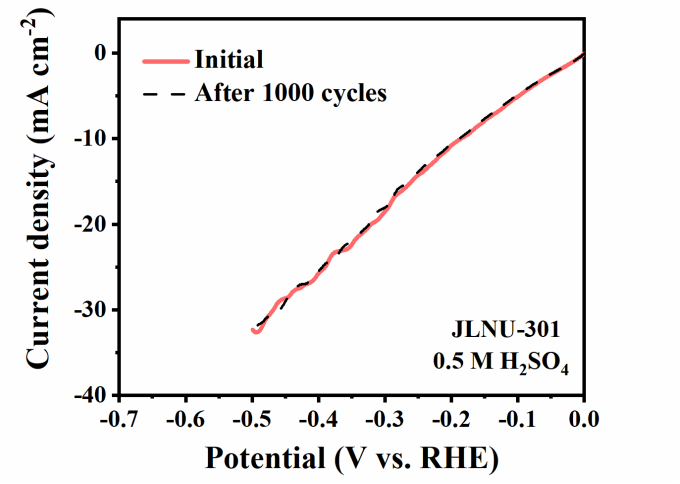

Figure S27. The LSV curves of JLUN-301 before and after 1000 CV tests.

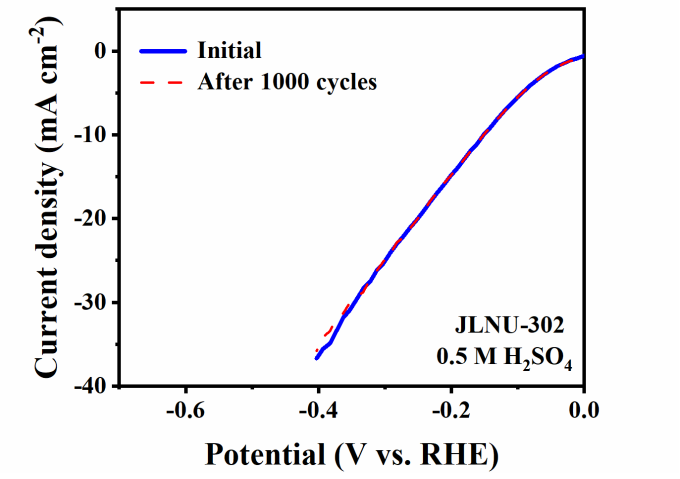

Figure S28. LSV curves of JLUN-302 before and after 1000 CV tests.

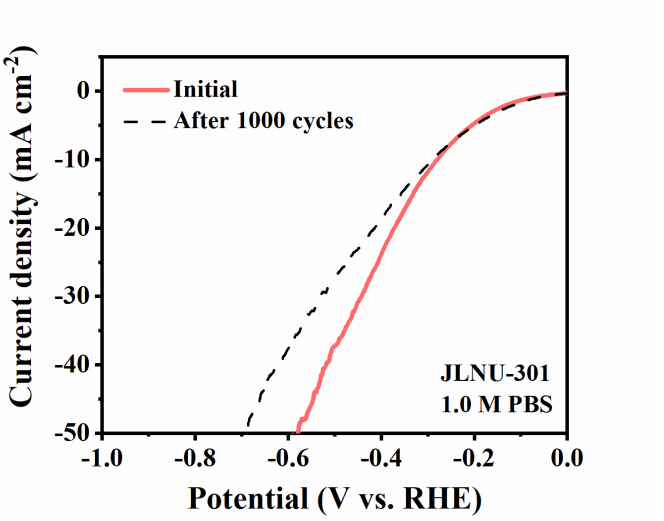

Figure S29. LSV curves of JLUN-301 before and after 1000 CV tests.

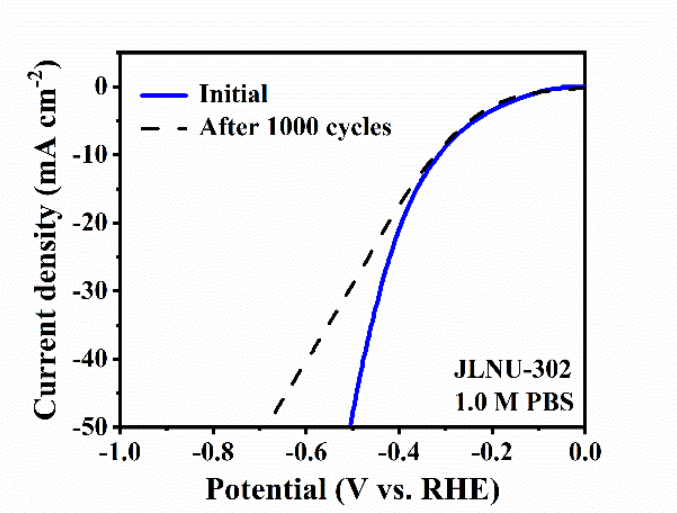

Figure S30. LSV curves of JLUN-302 before and after 1000 CV tests.

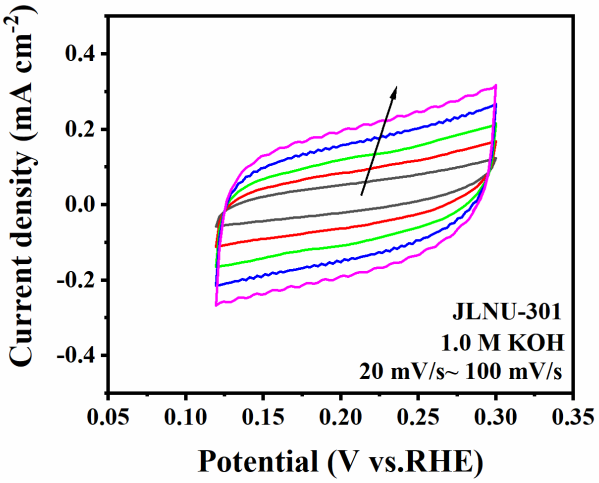

Figure S31. CV curves of JLNU-301 at different scan rates.

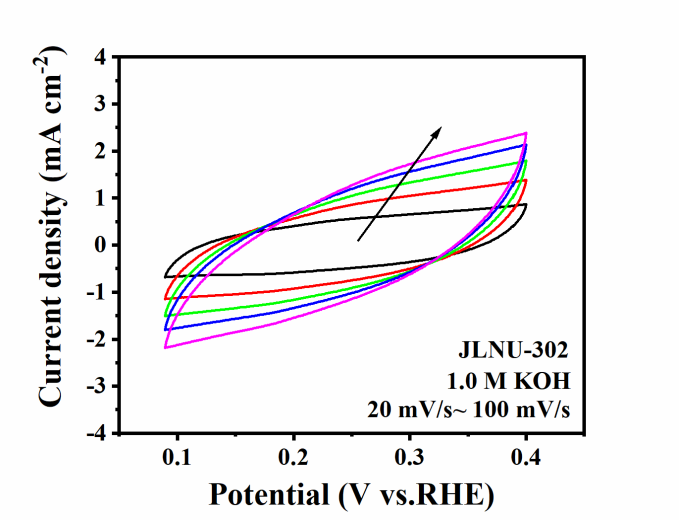

Figure S32. CV curves of JLNU-302 at different scan rates.

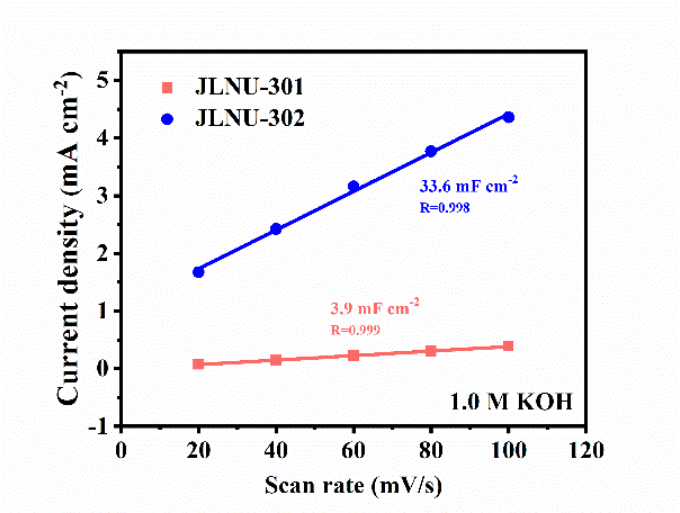

Figure S33. The C_{dl} plots for JLNU-301, and JLNU-302 at 1.0 M KOH.

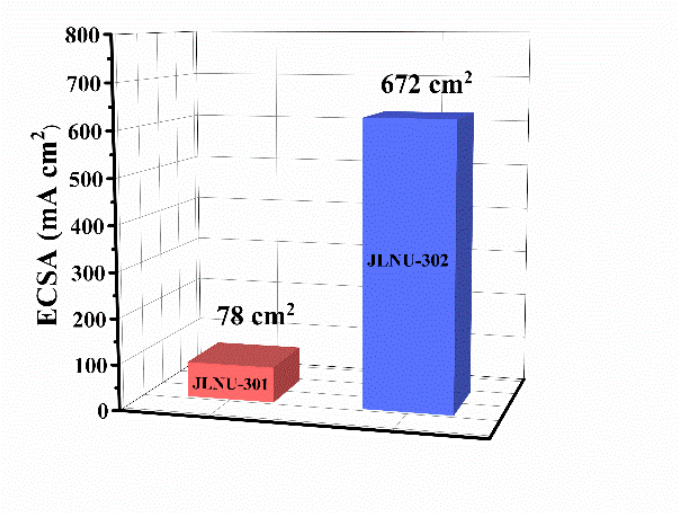

Figure S34. The ECSA for JLNU-301, and JLNU-302 in 1.0 M KOH.

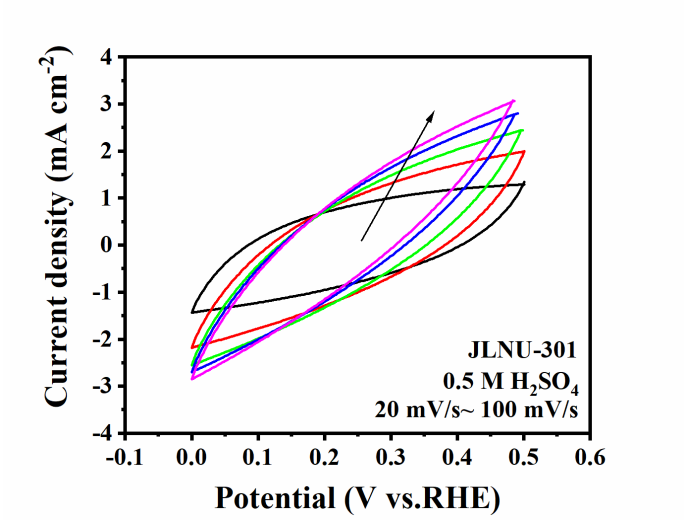

Figure S35. CV curves of JLNU-301 at different scan rates.

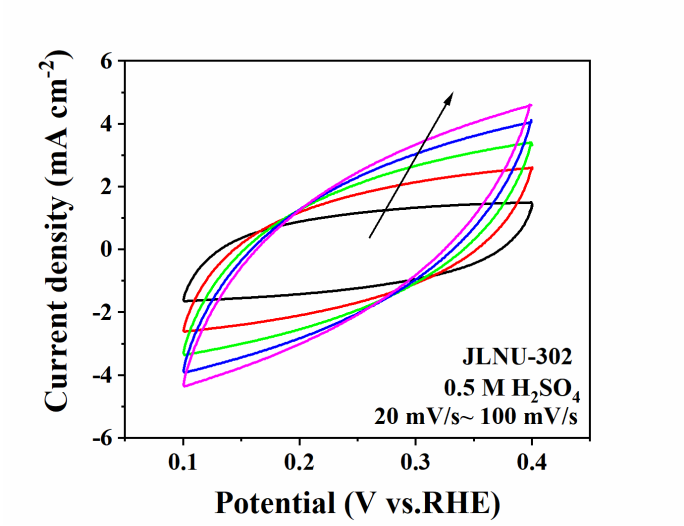

Figure S36. CV curves of JLNU-302 at different scan rates.

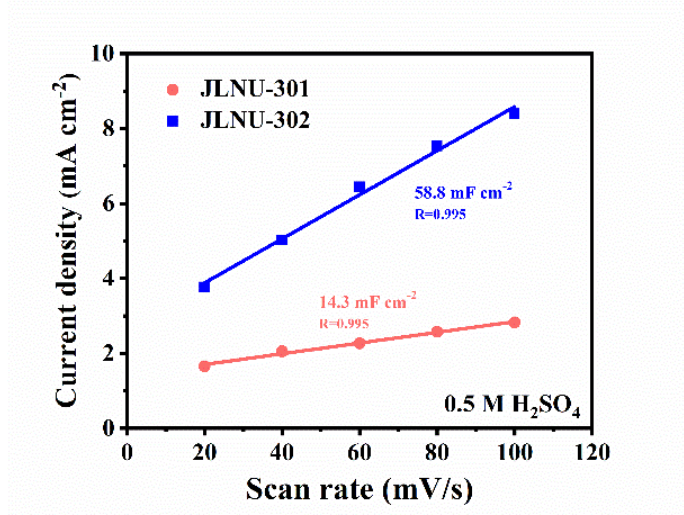

Figure S37. The C_{dl} plots for JLNU-301, and JLNU-302 at 0.5 M H_2SO_4.

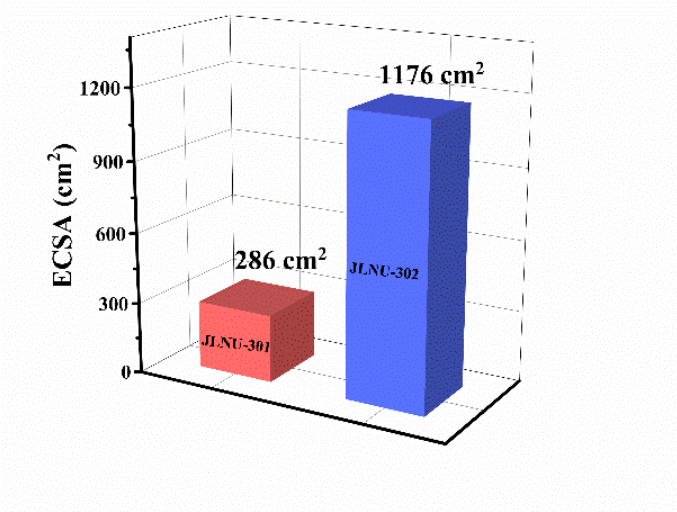

Figure S38. The ECSA plots for JLNU-301, and JLNU-302 at 0.5 M H_2SO_4.

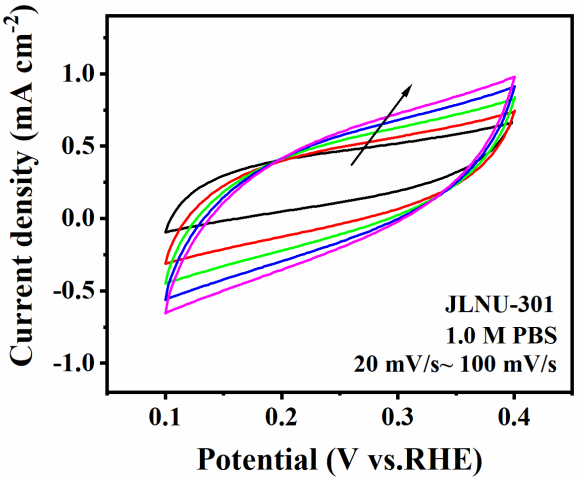

Figure S39. CV curves of JLNU-301 at different scan rates.

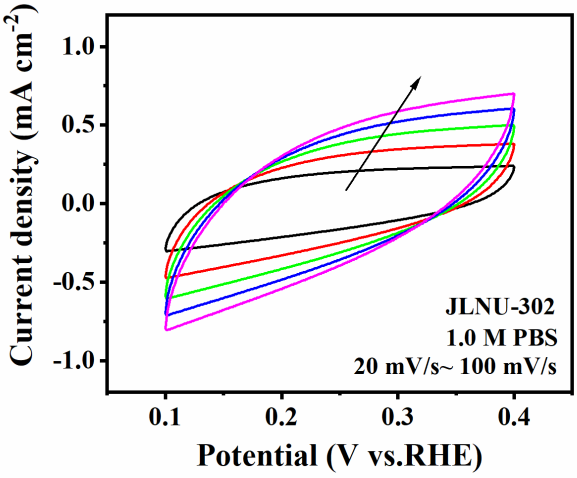

Figure S40. CV curves of JLNU-302 at different scan rates.

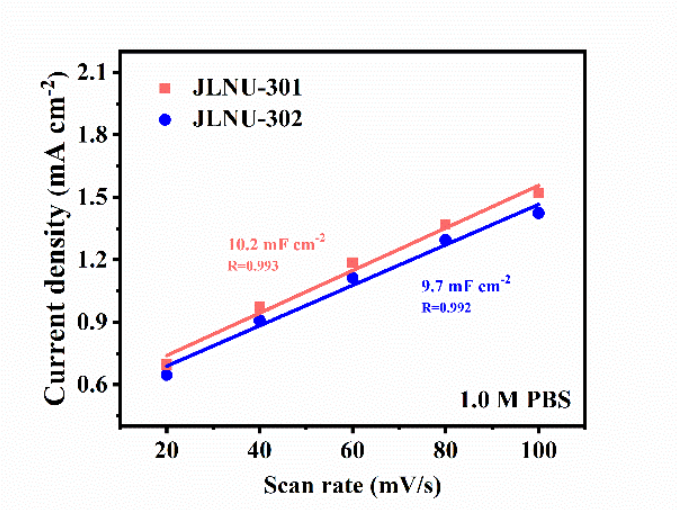

Figure S41. The C_{dl} plots for JLNU-301, and JLNU-302 at 1.0 M PBS.

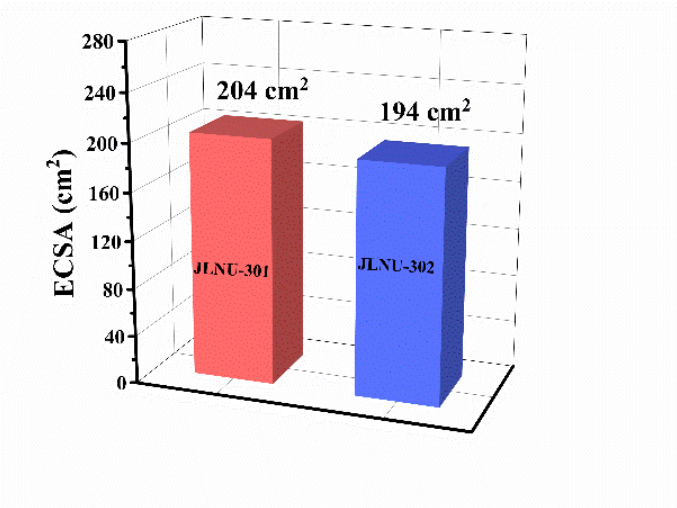

Figure S42. The ECSA plots for JLNU-301, and JLNU-302 at 1.0 M PBS.

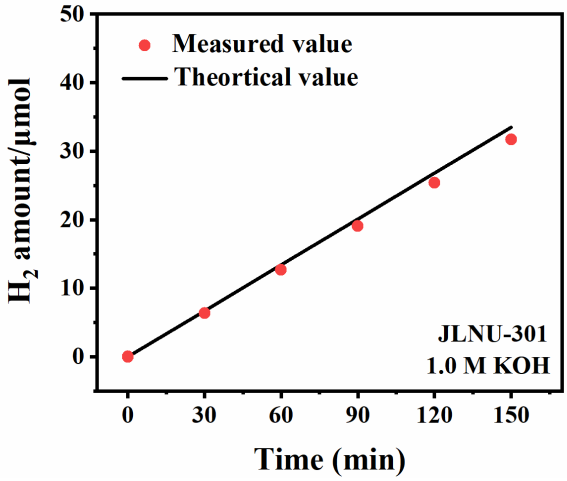

Figure S43. The Faraday efficiency for JLNU-301 in 1.0 M KOH.

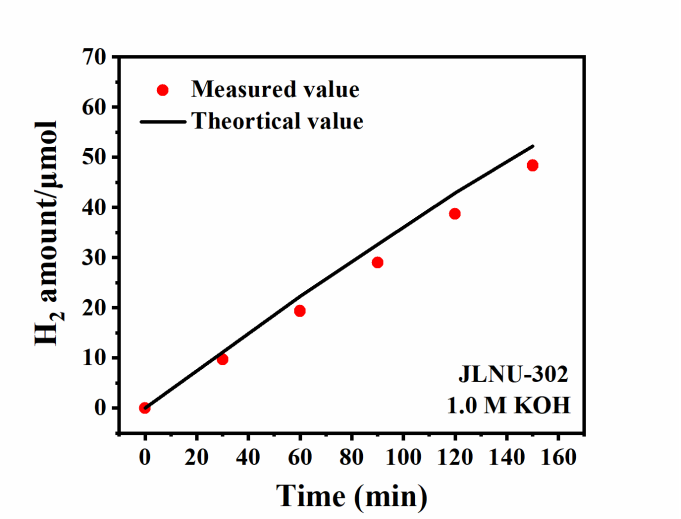

Figure S44. The Faraday efficiency for JLNU-302 in 1.0 M KOH.

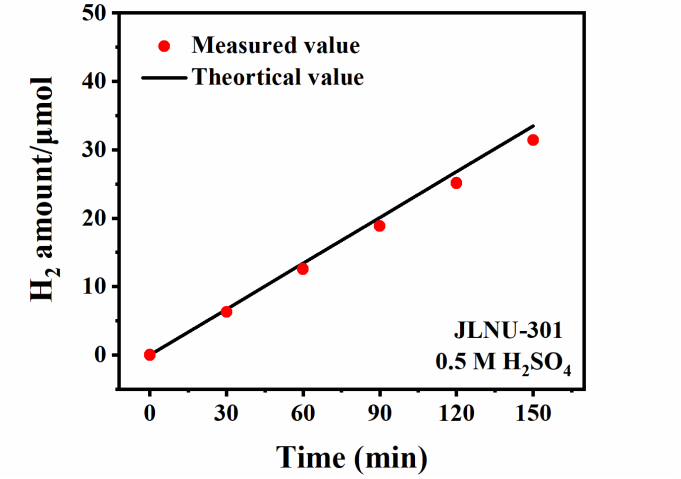

Figure S45. The Faraday efficiency for JLNU-301 in 0.5 M H_2SO_4.

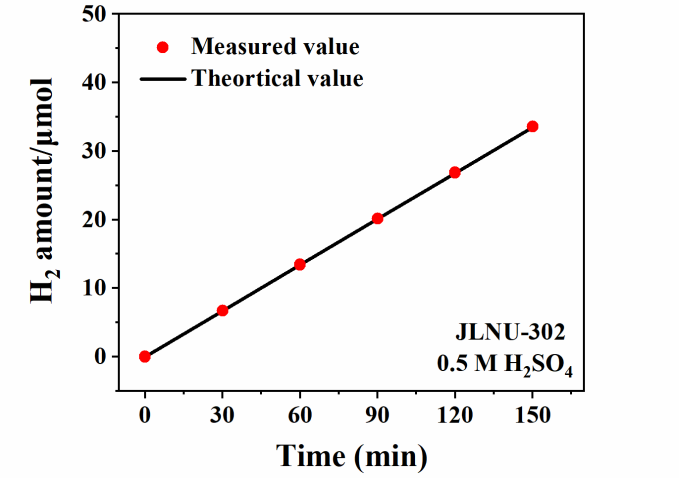

Figure S46. The Faraday efficiency for JLNU-302 in 0.5 M H_2SO_4.

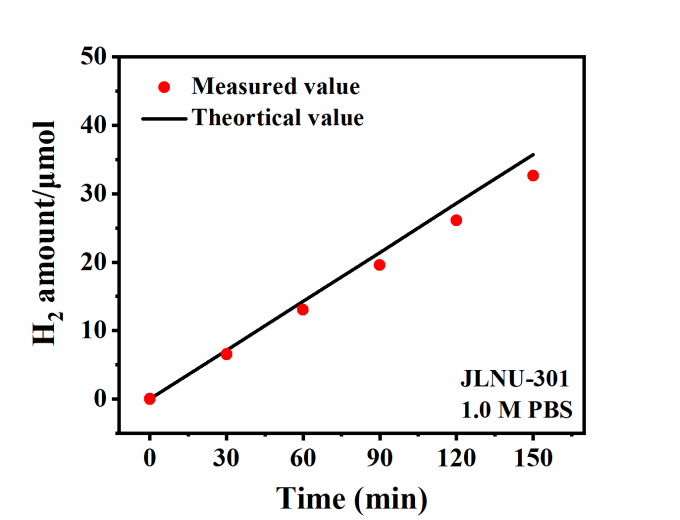

Figure S47. The Faraday efficiency for JLNU-302 in 1.0 M PBS.

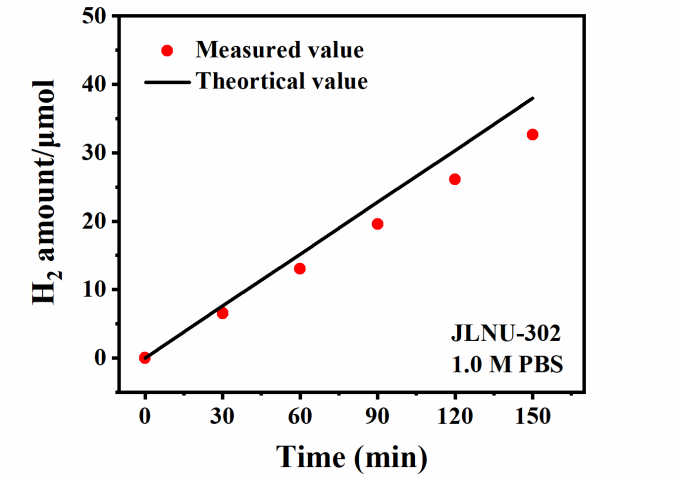

Figure S48. The Faraday efficiency for JLNU-302 in 1.0 M PBS

Section S8: Unit cell parameters and fractional atomic coordinates

Table S1. Unit cell parameters and fractional atomic coordinates for JLNU-301 calculated on the basis of staggered **hcb** net.

Space group		*P*6/M (No. 175)	
Calculated unit cell		a = b = 39.9400 Å, c =3.4967 Å, α= β = 90° γ= 120°	
Measured unit cell		a = b = 38.9714 Å, c = 3.4973 Å, α = β = 90° γ = 120°	
Pawley refinement		*R*ωp = 2.70% and *R*p = 1.87%	
Atom	x	y	z
C1	0.3551	0.6489	1
N2	0.37265	0.68831	1
C3	0.37864	0.62968	1
C4	0.41934	0.65185	1
C5	0.44169	0.63365	1
C6	0.42369	0.5931	1
C7	0.38292	0.57081	1
C8	0.3606	0.58902	1
N9	0.44741	0.57536	1
C10	0.43319	0.53804	1
C11	0.45859	0.52116	1
C12	0.499	0.54352	1
C13	0.48635	0.48112	1
S14	0.43964	0.47144	1
H15	0.43419	0.68493	1
H16	0.47477	0.65188	1
H17	0.36792	0.53772	1
H18	0.32751	0.5708	1
H19	0.40028	0.51826	1
H20	0.51378	0.5766	1

Table S2. Unit cell parameters and fractional atomic coordinates for JLNU-302 calculated on the basis of staggered **hcb** net.

Space group	*P*6/M (No. 175)
Calculated unit cell	a = b = 39.7190 Å, c = 3.5506 Å, α = β = 90° γ = 120°
Measured unit cell	a = b = 38.9714 Å, c = 3.4973 Å, α = β = 90° γ = 120°
Pawley refinement	*R*ωp = 1.13% and *R*p = 0.85%

Atom	x	y	z
C1	0.50575	0.48649	1
C2	0.48175	0.45002	1
C3	0.49915	0.43058	1
C4	0.53592	0.45289	1
C5	0.56149	0.43981	1
N6	0.5506	0.40574	1
C7	0.57464	0.39178	1
C8	0.56038	0.35457	1
C9	0.58314	0.34011	1
C10	0.62052	0.36272	1
C11	0.63482	0.40003	1
C12	0.61208	0.41451	1
C13	0.6445	0.34745	1
N14	0.68071	0.36943	1
S15	0.45002	0.50233	1
H16	0.45114	0.43556	1
H17	0.483	0.39998	1
H18	0.59159	0.45972	1
H19	0.53001	0.336	1
H20	0.57134	0.30975	1
H21	0.66516	0.41875	1
H22	0.62389	0.44488	1

Section S9: Comparison of HER performance with other electrocatalyst.

Table S3. Comparison of HER performance of JLNU-COFs with other electrocatalyst.

Catalyst	Overpotential 10 mA cm^{-2} (mV)			Reference
	Alkaline 1.0 M KOH	Acidic 0.5 M H_2SO_4	Netural 1.0 M PBS	
JLNU-301	136	189	282	**This work**
JLNU-302	91	151	320	**This work**
FeS/Fe_3C@N-S-C-800	446	174	798 (0.1 M PBS)	5
C-Fe,Co-COF	330	280	280	6
12%Ni@TPP-CB[6]	—	250	—	7
SB-PORPy	—	380 (5 mA cm^{-2})	—	8
Fe_2P@Fe_4N@C-800	—	232	—	9
TpPAM	—	250	—	10
FeTPP@NiTPP/NF	170	—	—	11
TiCP-PCP	—	142	—	12
N-HCNF-2-1000	—	243	—	13
1"-NP	—	260 (1.0 M $HClO_4$)	—	14
CTF@MoS_2-5	—	93	—	15
TQ-CMP	—	170	—	16
CoCOP	—	121	—	17
Pt@CTF-1	—	111	—	18
BPT-COF	—	142	—	19
CoP-2ph-CMP-800	360	—	—	20
NiCoFeP/C	149	—	—	21
Ni@NC_6-600	180	—	—	22

Section S10. References

[1] E. Skúlason, V. Tripkovic, M. E. Björketun, S. Gudmundsdóttir, G. Karlberg, J. Rossmeisl, T. Bligaard, H. Jónsson and J. K. Nørskov, *J. Phys. Chem. C*, **2010**, 114, 18182-18197.

[2] M. Chhetri, S. Maitra, H. Chakraborty, U. V. Waghmare, C. N. R. Rao, *Energy Environ. Sci*. **2016**, 9, 95-101.

[3] W. Sheng, A. Bivens M. Myint, Z. Zhuang, R. Forest, Q. Fang, J. Chen, Y. Yan, *Energy Environ. Sci.* **2014**, 7, 1719-1724.

[4] F. Rosalbino, S. Delsante, G. Borzone, E. Angelini, *Int. J. Hydrogen Energy* **2008**, 33, 6696−6703.

[5] T. Kong, X. Fan, A. Kong, Z. Zhou, X. Zhang, Y. Shan, *Adv. Funct. Mater.* **2018**, 28, 1803973.

[6] D. Wu, Q. Xu, J. Qian, X. Li, Y. *Sun. Chem. Eur.* J. **2019**, 25, 3105-3111.

[7] A. Khaligh, Y. Sheidaei, D. Tuncel, *ACS Appl. Energy Mater.* **2021**, 4, 3535-3543.

[8] S. Bhunia, S. K. Das, R. Jana, S. C. Peter, S. Bhattacharya, M. Addicoat, A. Bhaumik, A. Pradhan, *ACS Appl. Mater. Interfaces.* **2017**, 9, 23843-23851.

[9] X. Fan, F. Kong, A. Kong, A. Chen, Z. Zhou, Y. Shan, *ACS Appl. Mater. Interfaces*, **2017**, 9, 32840-32850.

[10] B. C. Patra, S. Khilari, R. N. Manna, S. Mondal, D. Pradhan, A. Pradhan, A. Bhaumilk, *ACS Catal*. **2017**, 7, 6120-6127.

[11] S. Yuan, L. Cui, X. He, W. Zhang, T. Asefa, *Int. J. Hydrog*. **2020**, 45, 28860-28869.

[12] A. Wang, L. Cheng, X. Shen, W. Zhu, L. Li, *Dyes Pigm*. **2020**, 181, 108568.

[13] Y. Zheng, S. Chen, H. Song, H. Guo, K. A. I. Zhang, C. Zhang, T. Liu, *Nanoscale* **2020**, 12, 14441-14447.

[14] C. Yang, S. Tao, N. Huang, X. Zhang, J. Duan, R. Makiura, S. Maenosono, *ACS Appl. Nano Mater*. **2020**, 3, 5481-5488.

[15] S. Qiao, B. Zhang, Q. Li, Z. Li, W. Wang, J. Zhao, X. Zhang, Y. Hu, *ChemSusChem*. **2019**, 12, 5032-5040.

[16] W. Wang, Y. Zhang, L. Chen, H. Chen, S. Hu, Q. Li, H. Liu, S. Qiao, *Polym. Chem.* **2021**, 12, 650-659.

[17] A. Wang, L. Cheng, W. Zhao, X. Shen, W. Zhu, J. *Colloid Interface Sci*. **2020**, 579, 598-606.

[18] M. Siebels, C. Schlüsener, J. Thomas, Y. Xiao, X. Yang and C. Janiak, *J. Mater. Chem. A*, **2019**, 7, 11934-11943.

[19] J. Chen, Y. Bai, Y. Liu, M. Liu, X. Wang, S. Shang, W. Gao, C. Du, Y. Qiao, J. Dong, Y. Liu, *Angew. Chem. Int. Ed.* **2021**, doi.org/10.1002/anie.202113067.

[20] H. Jia, Y. Yao, Y. Gao, D. Lu and P. Du, *Chem. Commun.* **2016**, 52, 13483-13486.

[21] X. Wei, Y. Zhang, H. He, L. Peng, S. Xiao, S. Yao, P. Xiao, *Chem. Commun*. **2019**, 55, 10896-10899.

[22] N. Cheng, N. Wang, L. Ren, G. Casillas-Garcia, N. Liu, Y. Liu, X. Xu, W. Hao, S. X. Dou, Y. Du, *Carbon,* **2020**, 163, 178-185.